

ORBITAL PARAMETERS FOR THE $250M_{\odot}$ ETA CARINAE BINARY SYSTEM

AMIT KASHI

Minnesota Institute for Astrophysics, University of Minnesota, 116 Church St. SE. Minneapolis, MN 55455, USA
and

Department of Physics, Technion – Israel Institute of Technology, Haifa 32000, Israel

NOAM SOKER

Department of Physics, Technion – Israel Institute of Technology, Haifa 32000, Israel

ABSTRACT

We show that recent observations of He I and N II lines of η Carinae may provide support for an orbital orientation where the secondary star is closest to us at periastron passages. This conclusion is valid both for the commonly assumed masses of the two stars, and for the higher stellar masses model where the very massive evolved primary star mass is $M_1 = 170M_{\odot}$ and its hot secondary star mass is $M_2 = 80M_{\odot}$. The later model better explains the change in the orbital period assuming that the ninetieth century Great Eruption was powered by accretion onto the secondary star. Adopting the commonly used high eccentricity $e \simeq 0.9$ and inclination $i = 41^{\circ}$, we obtain a good fit to newly released Doppler shift observations of He I emission and absorption lines assuming they are emitted and absorbed in the acceleration zone of the secondary stellar wind. Our model in which the secondary star is in the foreground at periastron is opposite to the view presented recently in the literature.

Keywords: (stars:) binaries: general—stars: mass loss—stars: massive —stars: individual (η Car)

1. INTRODUCTION

η Car is a binary system (Damineli 1996; Damineli et al. 1997) composed of a very massive primary star (Davidson & Humphreys 1997) and a hotter and less luminous evolved main sequence secondary star. Despite two decades of detailed observations (e.g., Smith et al. 2000; Duncan & White 2003; Whitelock et al. 2004; Corcoran 2005; Davidson et al. 2005, 2015; Smith 2006; Hamaguchi et al. 2007; Damineli et al. 2008b; Corcoran et al. 2010; Martin et al. 2010; Mehner et al. 2010, 2012, 2015; Abraham et al. 2014; Hamaguchi et al. 2014a,b) and modelling (e.g., Pittard et al. 1998; Soker 2001; Pittard & Corcoran 2002; Akashi et al. 2006, 2013; Kashi & Soker 2009a; Okazaki et al. 2008; Smith 2010; Groh et al. 2012; Madura et al. 2013, 2015; Clementel et al. 2015b) there are disagreements over two important properties of the binary system. These are the masses of the two stars and the orientation of the eccentric orbit.

The low-masses model assumes that η Car is at its Edington luminosity limit and a mass of $> 120M_{\odot}$ is derived (Hillier et al. 2001). Some studies take it to be the mass of the primary star, while other assumes that the combined masses of the two stars amounts to that mass with $M_1 \geq 90M_{\odot}$ and $M_2 \geq 30M_{\odot}$ (e.g., Okazaki et al. 2008; Clementel et al. 2015b).

The high-masses model was developed by us (Kashi & Soker 2010a) under the assumption that most of the extra energy released during the 1837–1856 Great Eruption (GE) of η Car originated from high accretion rate onto the secondary star. There are models that explain the GE with only one star (e.g., Matt & Balick 2004), and others that use three stars (Livio & Pringle 1998; Portegies Zwart & van den Heuvel 2016).

The GE was agiant eruption and a SN Impostor, which is the group of eruptive massive stars within the more general groups of intermediate luminosity optical transients (ILOTs; Kashi & Soker 2015). In Kashi & Soker (2015) we presented the high-accretion-powered ILOTs (HAPI) model, according to which all ILOTs are powered by high accretion rate onto a main sequence (MS), or a star slightly evolved off the MS (Kashi & Soker 2010b). According to the HAPI model,

kashi@astro.umn.edu

soker@physics.technion.ac.il

then, the luminosity peaks of the Great Eruption resulted from accretion onto the companion close to periastron passages. Those peaks are ≈ 5.1 – 5.2 years apart. If one assumes that the peaks are related to periastron passage, and occur about the same time after (or before) periastron, the separation between the peaks can be inferred as the orbital period. The second peak came after the eruption has started, and mass was lost. Therefore the orbital period is smaller than the time interval between the peaks. We adopted a value of 5.1 years. The present orbital period is 5.54 years, suggesting that during the Great Eruption the orbital period has increased. The orbital period changed as the secondary accreted mass, and as mass was lost from the binary system, both as a wind from the primary star and as jets from the secondary star.

In that study (Kashi & Soker 2010a) we found that for the HAPI mechanism to work within the orbital changes constraints, the two stars should have a significantly larger masses than $120M_{\odot}$. The masses should be in the range of $M_1 \simeq 150$ – $200M_{\odot}$ and $M_2 \simeq 60$ – $90M_{\odot}$. This high-masses model is further supported by evolution of massive stars on the HR diagram. The calculations of Figer et al. (1998) show that a zero-age main sequence (ZAMS) star with an initial mass of $M_{\text{ZAMS}} \simeq 230M_{\odot}$ is required to explain the present luminosity of the primary of η Car. Indeed, modern stellar evolution tracks of $120M_{\odot}$ stars even when rotation is considered (Ekström et al. 2012; Georgy et al. 2012) do not reach that luminosity, and more massive models of $M_{\text{ZAMS}} \simeq 250M_{\odot}$ are required, as found by Chen et al. (2015). The primary lost large amounts of mass to the bipolar nebula around η Car, the Homunculus (Smith & Ferland 2007; Gomez et al. 2010). When the large mass loss along the evolution is considered, a present mass of ~ 150 – $200M_{\odot}$ is compatible with the ZAMS mass inferred above.

In the debate on the orientation of the binary system, the two sides are holding a literally $\sim 180^{\circ}$ opposite views. One side holds that during periastron passages the primary star is closer to us ($\omega \simeq 240^{\circ}$ – 270° ; e.g., Iping et al. 2005; Nielsen et al. 2007; Damineli et al. 2008b; Henley et al. 2008; Parkin et al. 2009; Groh et al. 2010; Gull et al. 2011; Madura et al. 2012; Clementel et al. 2015a; Richardson et al. 2015; Teodoro et al. 2016, while the other side holds the view that during periastron passages the secondary star is at its closest location to us ($\omega \simeq 90^{\circ}$; e.g., Abraham et al. 2005; Falceta-Gonçalves et al. 2005; Abraham & Falceta-Gonçalves 2007; Kashi & Soker 2008, 2009b, 2011; Tsebrenko et al. 2013).

The disagreement on the orientation stems mainly from the controversy on the source of some emission and absorption lines, in particular the He I lines. In

a recent paper Richardson et al. (2015) present a study of the variations of some spectral lines with the phase of the binary orbit, based on observations with the CTIO 1.5m telescope. They attributed the He I lines to the primary star. In Kashi & Soker (2007), on the other hand, we assumed that the He I lines observed by Nielsen et al. (2007) are formed in the acceleration zone of the wind blown by the secondary star. We calculated the Doppler shift variations of the lines as a function of orbital phase with the low-masses model of η Car, and found that a good fit is obtained if the He I lines are formed in the region where the secondary wind speed is $v_{\text{zone}} = 430 \text{ km s}^{-1}$.

In the present study we combine the high-masses model of η Car with the assumption that the He I lines originate in the acceleration zone of the secondary stellar wind, and try to fit the new Doppler shifts presented by Richardson et al. (2015).

2. THE CONTROVERSY OF THE HELIUM I LINES

The origin of the visible He I P Cyg lines ($\lambda 7065\text{\AA}$, $\lambda 5876\text{\AA}$, $\lambda 5015\text{\AA}$, $\lambda 4992\text{\AA}$, and $\lambda 4471\text{\AA}$) in the binary system η Car is in dispute, with different researchers attributing it to different regions, e.g., the primary star (e.g., Falceta-Gonçalves et al. 2007; Humphreys et al. 2008; Richardson et al. 2015). We attribute the He I P Cyg lines to the acceleration zone of the secondary’s wind (Kashi & Soker 2007, 2008). A similar dispute exists for the N II $\lambda\lambda 5668$ – 5712\AA line (Mehner et al. 2011a). While Mehner et al. (2011a) argued that it cannot come from the secondary star, we noted that the N II lines closely follow the behavior of the He I lines, and attributed it to the secondary wind (Kashi & Soker 2011).

The effective temperature of the secondary was estimated by $T_{\text{eff},2} \sim 34\,000$ – $38\,000$ K by Verner et al. (2005), and more recently $T_{\text{eff},2} \sim 40\,000$ by Mehner et al. (2010). The main arguments for the He I P Cyg lines origin in the acceleration zone of the wind blown by the secondary star are as follows (Kashi & Soker 2011).

1. The Doppler shift of the P Cyg absorption components follows very well the secondary’s orbit, as we show in section 3 for the high-masses model, and as was shown before for the low-masses model (Kashi & Soker 2007, 2008).
2. The lines are known to originate in stars with temperatures well above 30000 K, mostly in hydrogen deficient stars (e.g., Leuenhagen et al. 1996; Crowther & Bohannan 1997; Grunhut et al. 2013; Wessolowski et al. 1988; Leuenhagen & Hamann 1998; further discussion is in section 5).

3. The secondary can account for the amount of absorption in the He I lines, as we show in section 4.
4. The Doppler shift of the emission follows that of the absorption, as we show in section 3.

The secondary mass loss rate is much lower than the primary's. It is important to mention that most of the lines observed from the η Car system do originate in the primary and its wind (the best example is probably the hydrogen lines; Weis et al. 2005, Davidson et al. 2005). Take H I $\lambda 4103\text{\AA}$ line for example. This line, and many others, originate in the primary. But it shows a P Cyg profile that shifts much less in periastron compared to the He I P Cyg lines we discuss here.

It might seem a “strange” coincidence that the place in the secondary wind where the He I are formed, according to our model, has about the same velocity as the primary's wind. However, even a stranger coincidence exists for a model where the lines are formed in the primary's wind: the area that absorbs the lines would have to change its velocity in the same way the secondary moves around the center of mass of the binary system.

Using the assumption that the He I lines originate in the secondary wind, in the past we fitted their Doppler shift variations with orbital phase for the low-masses model (the conventional model) of η Car, with $M_1 = 120M_{\odot}$ and $M_2 = 30M_{\odot}$ (Kashi & Soker 2008). The Doppler shift of the P Cyg absorption component of the He I lines was found to be in agreement with the binary orientation with a longitude angle $\omega = 90^\circ$, i.e., secondary closest to us at periastron. We here upgrade the model to include the new Doppler shifts presented recently by Richardson et al. (2015), and the high-masses model that better fits the luminosity and the behavior of η Car during the Great Eruption according to the HAPI model.

In fitting the He I lines Doppler shifts with orbital phase we scan the following parameter space.

1. The eccentricity is $e \simeq 0.85\text{--}0.93$.
2. Inclination angle (the angle between a line perpendicular to the orbital plane and the line of sight) is also in the consensus to be $i \simeq 41^\circ$.
3. The orbital period is $P = 2023$ days (Damineli et al. 2008a).
4. For the masses we use our results (Kashi & Soker 2010a) that the present masses are $M_1 \simeq 150\text{--}200M_{\odot}$ and $M_2 \simeq 60\text{--}90M_{\odot}$. We take here for the present masses of η Car components $M_1 = 170M_{\odot}$ and $M_2 = 80M_{\odot}$.

5. We assume that the observer is behind the secondary at periastron, namely $\omega \simeq 90^\circ$.

We note that there is inconsistency in some papers regarding the exact epoch of periastron, or phase 0. Richardson et al. (2015) used JD 2454842.5 for the 2009 periastron passage. Mehner et al. (2011a) used JD 2454860 as a reference time for the event (see also discussion at the appendix of Mehner et al. 2011b). The uncertainty in determining the time of periastron may cause the change in radial velocity to appear after periastron rather than before, or vice versa. Evidently the observations collected so far from η Car are insufficient for determining the exact time of periastron. We will adopt an intermediate value between the references above, $t_{\text{per}} = \text{JD } 2454850$. This value coincides with having the sharp variation in radial velocity of the lines studied here at periastron. However, one should bear in mind that the uncertainty of the periastron epoch is of ± 10 days. We corrected the orbital phases inferred from the observation dates in this work to have phase 0 at t_{per} .

3. ORBITAL PARAMETERS

Based only on geometric considerations, i.e., neglecting variations of the wind speed near periastron passage and stochastic wind speed variations, we here use our model to fit the observations of Richardson et al. (2015). The orbital velocity of the secondary relative to the primary, v_{orb} , is converted to the velocity relative to the center of mass

$$v_m = \frac{M_1}{(M_1 + M_2)} v_{\text{orb}} = \left[\frac{G^{1/2} M_1}{(M_1 + M_2)^{1/2}} \right] \left[\frac{2}{r(t)} - \frac{1}{a} \right]^{1/2}, \quad (1)$$

that can be written as

$$\begin{aligned} v_m &= \left[\frac{M_1}{(M_1 + M_2)^{2/3}} \right] \left[\frac{2\pi G}{P} \right]^{1/3} \left[\frac{2}{\tilde{r}(t)} - 1 \right]^{1/2} \\ &= f_M \left[\frac{2\pi G}{P} \right]^{1/3} \left[\frac{2}{\tilde{r}(t)} - 1 \right]^{1/2}. \end{aligned} \quad (2)$$

where $\tilde{r}(t) \equiv r(t)/a$.

The entire stellar mass dependency is embedded in the factor f_M . For the low-masses model ($M_1 = 120M_{\odot}$ and $M_2 = 30M_{\odot}$) its value is $f_M = 4.25M_{\odot}^{1/3}$, while for the high-masses model ($M_1 = 170M_{\odot}$ and $M_2 = 80M_{\odot}$) it is $f_M = 4.28M_{\odot}^{1/3}$. Therefore the amplitude of the fit with the new parameters is less than 1% larger than the amplitude using the old parameters.

On top of v_m there are factors related to the observation angle ω , the inclination i , and the eccentricity e . From the result we subtract the constant velocity v_{zone} of the zone in the secondary wind where the lines are absorbed, or the average velocity of the emitting gas when

the peak emission is fitted. Figure 1 shows in a blue-solid line our fit to the observed radial velocity absorption component of He I lines from Richardson et al. (2015) and of Nielsen et al. (2007). It is clear from Figure 1 that our fit to the new lines at $\lambda 4922\text{\AA}$ and $\lambda 5015\text{\AA}$ is not as good as our fit to the lines studied by Nielsen et al. (2007). We attribute this to contamination of the two $\lambda 5015\text{\AA}$ and $\lambda 4922\text{\AA}$ lines by Fe II lines. This contamination was mentioned by Richardson et al. (2015).

More observations of He I lines, specifically the He I $\lambda 4714\text{\AA}$ line, were taken for the 2009 event by Mehner et al. (2011b), and for the 2014.6 event by Mehner et al. (2015). The later paper summarizes observations of that line from the previous 3 events (2003.5, 2009, and 2014.6). Figure 2 shows how our model fits the observations. We used the same model we used for the other He I lines in Figure 1, but $v_{\text{zone,abs}} = 370 \text{ km s}^{-1}$. We take this slightly different value than the value of $v_{\text{zone,abs}} = 430 \text{ km s}^{-1}$ that was used in Figure 1 to match the average of the absorption component’s radial velocity. The different values mean either that the He I $\lambda 4714\text{\AA}$ line is absorbed in the wind slightly closer to the wind origin on the secondary star, or that there are large variations and uncertainties in the derived Doppler shifts near periastron passages.

Mehner et al. (2015) found that the 2014.6 event was different than previous events, and according to their interpretation in the framework of the accretion model, it showed signs of less accretion onto the secondary close to periastron, indicating weaker primary wind. The He I line flux increased significantly in 2009–2014 compared to 1998–2003. The absorption of the He I $\lambda 4714\text{\AA}$ line disappeared 8 days before periastron and re-appeared 8 days after (assuming our t_{per}). The radial velocities are lower in the 2014.6 event compared to previous events. In fact, for fitting only the data from 2014.6 it would be better to use $v_{\text{zone,abs}} = 330 \text{ km s}^{-1}$, keeping the rest of the parameters unchanged. This behavior, together with the large fluctuations in the Doppler shifts near periastron as seen in the different figures, suggest that the velocities of the regions where lines are formed in the different regions of the secondary wind vary from cycle to cycle and in short time scales near periastron passages. We should therefore aim at fitting the general behavior of the Doppler shift variations with orbital phase; a perfect fit to the Doppler shifts of this interacting binary system cannot be achieved using the geometrical effects alone.

We used the same principles we used for fitting the radial velocity variations of the He I absorption lines to fit the emission peak bisector velocity of the He I $\lambda 6678\text{\AA}$ line across the 2009 event observed by Richardson et al. (2015). We find that a value of $v_{\text{zone,emi}} = 60 \text{ km s}^{-1}$ for the average velocity of the gas emitting the line

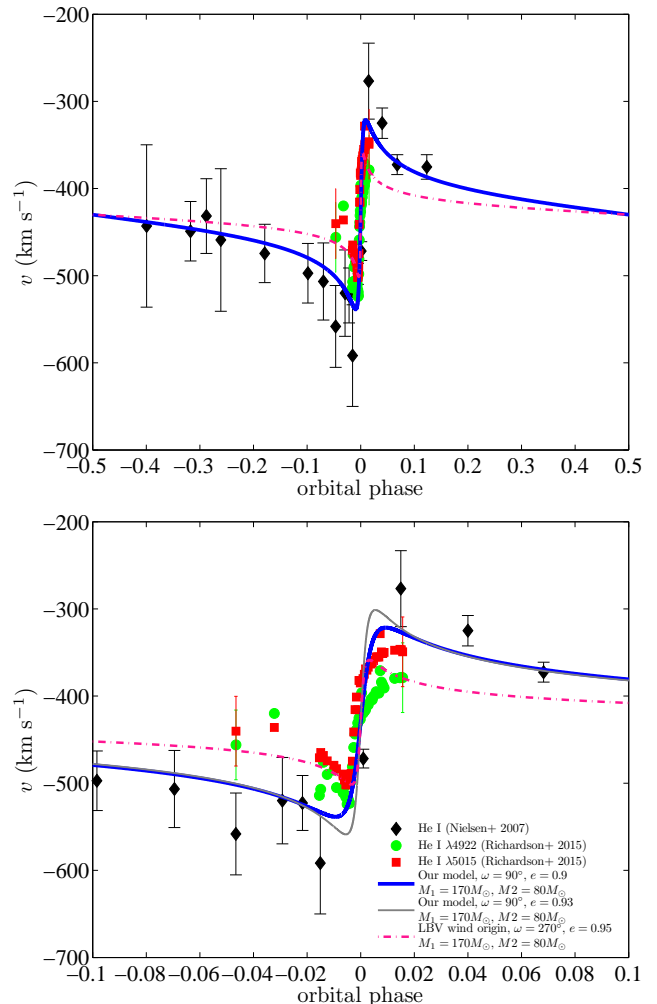


Figure 1. Our fit to the observed radial velocity absorption component of He I lines. The black diamond points are the He I $\lambda 7065\text{\AA}$, $\lambda 5876\text{\AA}$, $\lambda 5015\text{\AA}$, $\lambda 4992\text{\AA}$, and $\lambda 4471\text{\AA}$ lines from Nielsen et al. (2007) with the original error bars. The CTIO radial velocity data from Richardson et al. (2015) are shown in green circles (He I $\lambda 4922\text{\AA}$) and red squares (He I $\lambda 5015\text{\AA}$), and include no error bars. We added bars to two points of each set that indicate our estimate of the fluctuations in the velocity of the wind absorption component, $\pm 40 \text{ km s}^{-1}$. Observation phase was modified to periastron time defined in the text. Our fiducial model assumes that the spectral lines originate in the secondary stellar wind, that $\omega = 90^\circ$ (i.e., secondary star closest to us at periastron), an eccentricity of $e = 0.9$, and stellar masses of $M_1 = 170M_\odot$ and $M_2 = 80M_\odot$. The upper panel shows the entire orbit, and the bottom panel is zoomed to times near periastron. The lower panel includes also a model with $e = 0.93$ instead of $e = 0.9$ (grey line). For comparison we present a fit for a case where the He I lines originate from the primary stellar wind, and the orientation is $\omega = 270^\circ$ (dashed-dotted pink line). The velocity of the region in the wind responsible for the lines is taken to be $v_{\text{zone,abs}} = 430 \text{ km s}^{-1}$.

gives the best results. Figure 3 shows the fit we obtained, together with the observations of the emission peak bisector velocity of the He I $\lambda 6678\text{\AA}$. We present two other cases with $\omega = 90^\circ$ (secondary star closer to

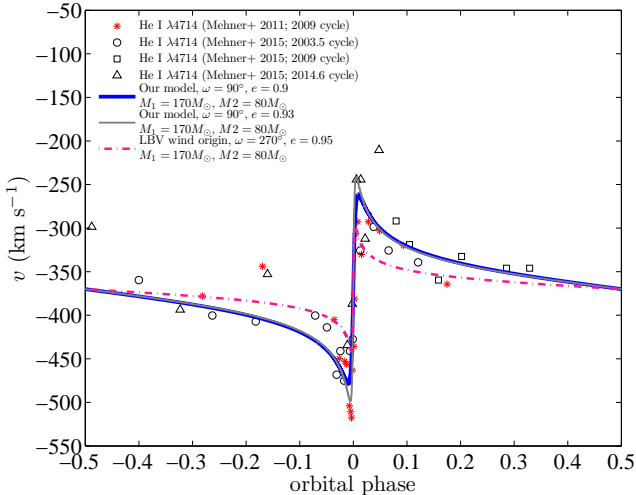


Figure 2. Like Figure 1, but taking $v_{\text{zone,abs}} = 370 \text{ km s}^{-1}$ to fit the observed radial velocity absorption component of the He I $\lambda 4714 \text{ \AA}$ line, from observations of Mehner et al. (2011b) and Mehner et al. (2015).

the observer at periastron), one with an eccentricity of $e = 0.93$, and the other is the low-masses model from Kashi & Soker (2008). We also show two models where the line is assumed to originate in the primary stellar wind. One is our simple geometric model, but the line is emitted by the primary stellar wind and $\omega = 270^\circ$ (dashed-dotted line), and the second is the fit presented by Richardson et al. (2015). It is clear that the models where the line is emitted by the secondary stellar wind and the secondary star is in the foreground at periastron result in a much better fit to the observations.

We next test our model against the variation in the Doppler shift of the absorption component of the N II $\lambda 5666\text{--}5771 \text{ \AA}$ lines, taken from both Richardson et al. (2015) and Mehner et al. (2011a). We use here $v_{\text{zone,abs}} = 370 \text{ km s}^{-1}$. The N II $\lambda 5668 \text{ \AA}$ line observed by Mehner et al. (2011a) has clear emission peaks close to periastron, but these were not clear in the profiles of Richardson et al. (2015). We fit also the emission component of the N II $\lambda 5668 \text{ \AA}$ line, with $v_{\text{zone,emi}} = 70 \text{ km s}^{-1}$. The fits are presented in Figure 4.

Though the N II and He I lines intensities behave differently, the radial velocity of the N II $\lambda 5668 \text{ \AA}$ emission component follows that of the absorption component amazingly well. Also, the entire lines-formation regions show the same Doppler shift variation. Such a behavior cannot be explained in frame of a model where the N II and He I lines-formation regions change their location within the primary wind.

The main driver of the variations in the Doppler shifts is the pure orbital motion. However, it is not the only one. A variation in location within the secondary wind in our model can take place, and it is even expected to

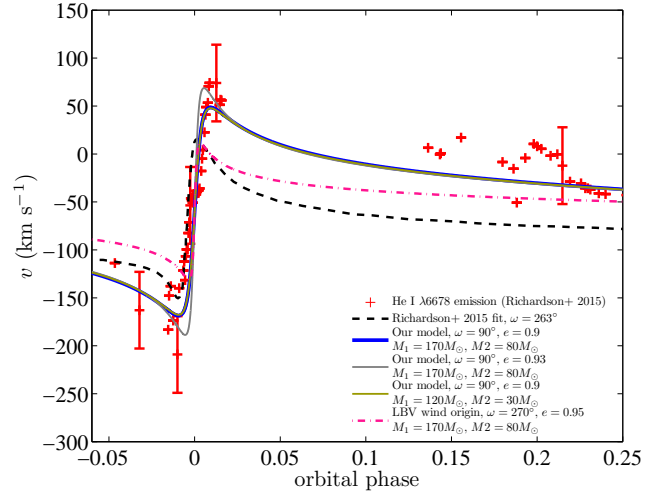


Figure 3. Our fit to the emission peak bisector velocity of the He I $\lambda 6678 \text{ \AA}$ line (blue line). We show also the low-masses model (yellow line), and a higher eccentricity model (grey line). Bars indicate our estimate of fluctuations in the average velocity of the emitting gas in the secondary wind. Also shown is the case where the line originates in the primary stellar wind and the primary star is closest to us at periastron (dashed-dotted pink line). The black dashed line is the fit to the data taken from Richardson et al. (2015), who assume that the line originates in the primary wind.

occur. As the secondary approached periastron, its wind properties change, most likely due to accretion of gas from the primary stellar wind (Soker 2005; Akashi et al. 2013). The accretion phase lasts for several weeks, but the influence on the secondary stellar wind properties can last few months after the event, until the accreted mass is removed by the restoring secondary wind (Kashi & Soker 2009). It is therefore very reasonable that lines will be absorbed in different locations across periastron. This secondary effect is the main cause for the deviation from our Doppler-based model, as seen in the figures.

4. ABSORPTION OF HELIUM BY THE SECONDARY

According to Nielsen et al. (2007) the amount of absorption of the He I $\lambda 5015 \text{ \AA}$ P Cyg line reaches up to 50%. This line, however, shows different orbital change (probably because it is blended) and is *not* one of the lines we claim to originate in the secondary wind (see section 3). The He I lines we attribute to the secondary, show much less absorption. The He I $\lambda 7067 \text{ \AA}$ P Cyg line, for example, shows 10% absorption near periastron Nielsen et al. (2007). We can use this to better constrain the properties of the two stars.

The maximum absorption, assuming it occurs in the secondary wind, is obtained when

$$A_{\text{max}} = \frac{f_{l2} L_2}{f_{l1} L_1 + f_{l2} L_2} \quad (3)$$

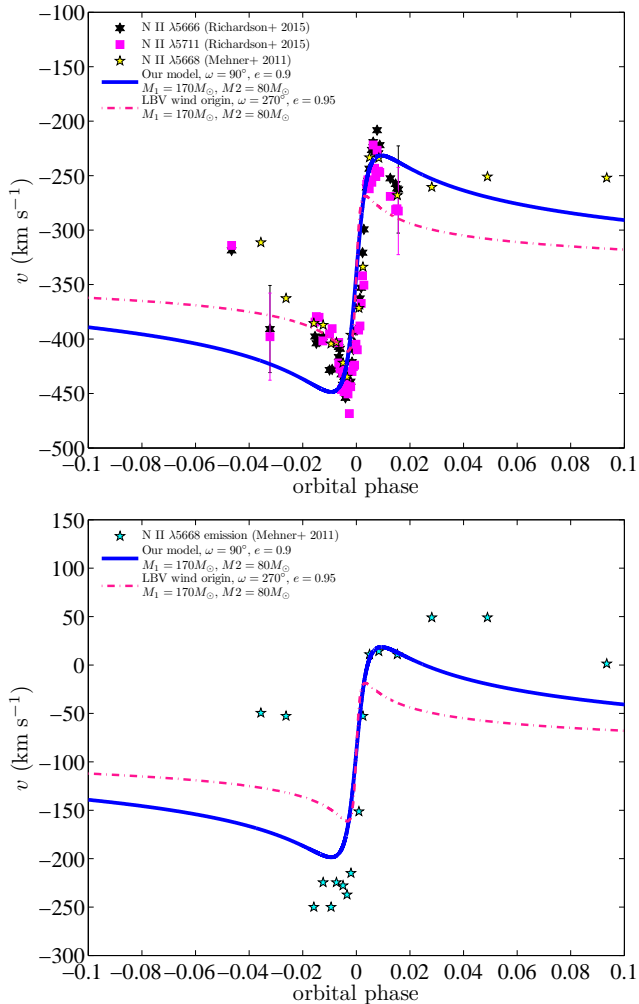


Figure 4. Upper panel: Our fit to the observed radial velocity absorption component of the N II $\lambda 5666\text{\AA}$ and N II $\lambda 5771\text{\AA}$ lines from the 2009 event (Richardson et al. 2015), and the N II $\lambda 5668\text{\AA}$ line observed by Mehner et al. (2011a) in the 3 previous events. Lower panel: Our fit to the observed radial velocity emission component of the N II $\lambda 5668\text{\AA}$ line from Mehner et al. (2011a).

Where L_1 and L_2 are the luminosities of the primary and the secondary, respectively, and f_{l_1} and f_{l_2} are their fractions within the line absorption waveband.

According to Nielsen et al. (2007), the He I $\lambda 7067\text{\AA}$ shows 10% absorption for a range between -700 – -500 km s^{-1} . Taking $A_{\text{max}} \leq 0.1$ in equation (3) we get the requirement that

$$\frac{f_{l_1} L_1}{f_{l_2} L_2} \leq 9. \quad (4)$$

Assuming Blackbody radiation, and taking conventional parameters for the temperatures of the primary and the secondary $T_1 = 20\,000\text{K}$ and $T_2 = 40\,000\text{K}$, respectively, we obtain $f_{l_1}/f_{l_2} = 5.9$. This means that according to equation (4), the luminosity ratio needs to satisfy $L_2/L_1 \geq 0.65$. According to the conventional parameters, the ratio $L_2/L_1 = 0.2$, so this leads to a contra-

diction. It is not possible to find for the conventional model, a point in the stellar evolution path, even with a different effective temperature, that would be even close to satisfy that requirement. We therefore conclude that the two stars must have a smaller luminosity ratio, and consequently smaller mass ratio, as is expected in the massive stars model. They should also have a smaller temperature ratio to make the requirement in equation (4) easier to meet.

For the massive stars model we propose, we can track the evolution of $M_1 = 170M_\odot$ and $M_2 = 80M_\odot$ stars (e.g., Ekström et al. 2012, Köhler et al. 2015 and references therein), and try to find a reasonable set of parameters that satisfies the above equation. We find that if we take $T_1 = 25\,000\text{K}$ (Hillier et al. 2001), $T_2 = 37\,000\text{K}$ (Verner et al. 2005), which gives $f_{l_1}/f_{l_2} = 2.8$, then the requirement from equation (4) becomes $L_2/L_1 \geq 0.31$. And indeed, stellar evolution tracks give $L_1 \simeq 3 \times 10^6 L_\odot$ and $L_2 \simeq 1.2 \times 10^6 L_\odot$, satisfying the condition.

5. SUMMARY AND DISCUSSION

We used spectroscopic observations of η Car close to the 2009 periastron passage (Richardson et al. 2015; Mehner et al. 2011a,2011b) to show they support earlier suggestions that companion is in the foreground at periastron (Kashi & Soker 2011 and references therein).

We assumed that the He I and N II spectral lines originate in the acceleration zone of the secondary star of η Car (Kashi & Soker 2007, 2011). We then took the secondary to be closest to us at periastron passages, i.e., $\omega = 90^\circ$. We further used the high-masses model of η Car with component masses of $M_1 = 170M_\odot$ and $M_2 = 80M_\odot$. These masses better fit evolutionary tracks of massive stars that cross the locations of the two stars on the HR diagram, than the commonly used masses of $M_1 = 120M_\odot$ and $M_2 = 30M_\odot$. A massive primary star with initial mass larger than $M_1 = 200M_\odot$, and a secondary star with an initial mass larger than $M_2 = 50M_\odot$ are supported by stellar evolution calculations for very massive stars (e.g., Yungelson et al. 2008; Brott et al. 2011; Yusof et al. 2013).

The high masses, more generally in the range of $M_1 \simeq 150$ – $200M_\odot$ and $M_2 \simeq 60$ – $90M_\odot$, can account also for the powering of the nineteenth century Great Eruption by mass accretion onto the secondary star (the HAPI model; Kashi & Soker 2010a). For the eccentricity and inclination angle we used the commonly accepted values of $e \simeq 0.9$ and $i = 41^\circ$, respectively. As evident from Figs. 1–4 we could fit the general variation of the Doppler shifts with orbital phase. Therefore, the suggestion that the secondary star is in the foreground at periastron (e.g., Kashi & Soker 2008; Tsebrenko et al. 2013) is definitely tenable. The suggestion that the primary star is in the foreground at periastron seems to

encounter problems, e.g., as evident from the dashed black line in Figure 2 that is the model proposed by Richardson et al. (2015).

In some cases the opposite model, of a line originating from the primary stellar wind and the primary star is in the foreground at periastron passages, might fit part of the Doppler shifts, e.g., fitting the data from Richardson et al. (2015) in Figure 1. However, this model has too low amplitudes both at periastron passages, as evident from all figures, and away from periastron passages, e.g., right side of Figure 2.

In the present study we considered only the role of the orbital motion on the variation of the Doppler shift with orbital phase. It appears clear from the fluctuations in the Doppler shift values and from the non-perfect fitting that the velocity of the zone responsible for the formation of each line is changing. Both stochastic variations and variation with orbital phase, noticeably near periastron passages, exist. These variations are another manifestation of the unrelaxed nature of this binary system.

The three unknowns about the binary system discussed here are: (i) masses of two stars; (ii) orbital orientation; (iii) exact periastron time. The masses of the two stars were obtained by Kashi & Soker (2010a) as explained in section 1. Here we showed that the mass estimate obtained by Kashi & Soker (2010a) also allows to fit radial velocities of the lines. The orbital orientation is the main parameter discussed here in detail. The time of periastron is uncertain. We used a fixed value here and did not fine-tune its value. It may however be possible to use the He I and other lines to get a better constrain for its time. What we find here is that our fits are consistent with periastron time of JD 2454850 but a few days difference is also possible.

In addition to the Doppler shifts presented here, there are other arguments that support the suggestion that the secondary star is in the foreground at periastron passages. The four supporting arguments listed by Kashi & Soker (2008) include the evolution of the radio emission and the behavior of the He I $\lambda 10830\text{\AA}$ line. In a previous study (Kashi & Soker 2009b) we further argued that the column density toward the X-ray emitting gas, that is the post-shock secondary wind, is more compatible with a binary orientation where for most of the time the secondary star is in the background, being on the foreground only near periastron passages. Another supporting argument was brought by Tsebrenko et al. (2013). They demonstrated that the asymmetric morphology of the blue and red-shifted components of the outflow at hundreds of astronomical units from η Car, can be accounted for from the collision of the free primary stellar wind with the slowly expanding dense equatorial gas closer to us. Namely, for most of the orbital

period the primary is in the foreground, and at periastron passages the secondary star is in the foreground.

Humphreys et al. (2008) discovered that the He I lines were absent from η Car’s spectra prior to the mid 1940s. They discussed the various difficulties it may pose to models attributing the required He ionizing photons to the secondary, ionizing the primary wind. They also conclude that even a much denser primary wind could not have obscured the He ionizing photons coming from the secondary. Clementel et al. (2015b) and Mehner et al. (2015) claimed, however, that the He ionizing photons only moderately penetrate the dense post-shocked primary wind. Therefore if the primary wind at that time was 2–4 times denser, it should have been enough to change the ionization structure of He in the primary’s wind, and prevent the formation of the lines. These arguments, however, are irrelevant for a model in which the He I lines originate in the secondary’s wind. In the frame of the accretion model, however, it is easier to provide an explanation. A denser primary wind can form a thick accretion belt around the secondary close to periastron (Kashi & Soker 2009) that would last for the entire orbit, providing a shield for its radiation. Even after the belt is gone, the mass that is accreted onto the secondary changes its photospheric structure and makes it cooler, diminishing the He ionizing photons. This may require that the primary wind before the 1940s was 20–30 times denser. A new study by Kashi et al. (2016) suggests that the mass loss could have reached that magnitude or even higher.

Mehner et al. (2011a) also observed the N II lines and their velocity shifts from reflected polar spectra at the location known as “FOS4”. They argue it may be a problematic observation for the orbital motion explanation to the Doppler shift variations. A similar argument appears in Mehner et al. (2011b) regarding the He I $\lambda 4714\text{\AA}$ line. The only direct comparison of FOS4 and direct view is in figure 8 of that paper. Though it may at first sight look like the radial velocity of the absorption in FOS4 follows that of the direct view, we notice the following: (1) The observations at -353 and -82 days (phase -0.18 and -0.045) show very high radial velocity in absorption, much above other observations of the same line. (2) At -82 days the value of FOS4 is 40 km s^{-1} higher. As the observations are sparse, there is now way to know if this is significant. It may indicate that the FOS4 Doppler shift of the absorption is smaller in amplitude and non systematic. Alternatively, it may be a fluctuation. It is therefore impossible to know if FOS4 persistently follows the direct view or not. A detailed comparison of densely sampled multiple lines is needed in order to check that. Even if it does, it may well be possible that not only polar light is reflected to FOS4 and there is some reflection from equatorial regions.

Mehner et al. (2010) used the distribution of gas and ionizing radiation around η Car to constrain the properties of the secondary. If the limits of Mehner et al. (2010) hold, then the secondary mass should be $M_2 \lesssim 60M_\odot$. A mass of $M_2 = 60M_\odot$ is still within the HAPI model for the Great Eruption. We here showed that the Doppler shifts can be fitted with $M_2 = 30M_\odot$ and $M_2 = 80M_\odot$. Any value for M_2 in this range can be fitted. But as stated, because of the luminosity of the primary star and the HAPI model for the GE, we prefer the high-masses model.

P Cyg profiles in He I are found in hot hydrogen poor stars (Leuhenagen et al. 1996; Wessolowski et al. 1988; Leuhenagen & Hamann 1998). We know from observations that the primary's outer layers consists of about 50% helium (Davidson et al. 1986; Dufour et al. 1997). A few M_\odot of material from the primary were accreted onto the secondary during the eruptions. The accreted gas makes the secondary's envelope enriched with helium. It is very plausible that even though the secondary is hot, its helium lines are stronger than other stars in its evolutionary stage. Clumpiness of the secondary wind (Kashi & Soker 2007) can make part of the gas somewhat cooler, also enhancing the He I lines.

The very massive primary star of $M_1 > 150M_\odot$ and

the very high eccentricity of the binary orbit hints that the system was once a triple system, and that the primary formed by the merger of two (or more) stars. The merger process released large amount of gravitational energy within weeks to months. Such an event can be classified as ILOT. Therefore, it may well be that the nineteenth century Great Eruption was not the first ILOT of this system. We note that the estimates for the masses in the HAPI model do not depend on the previous existence or nonexistence of a third star. The masses of only two stars are relevant for both the calculations done in this paper for spectral fitting, and the calculation done in Kashi & Soker (2010a) for modeling the light curve. The third star is suggested as a possible easier route to obtain the large mass of the primary, together with a high eccentricity orbit. But it is well possible that both were obtained with only two stars along the entire evolution.

AK acknowledges support provided by National Science Foundation through grant AST-1109394. We thank Roberta Humphreys, Kris Davidson, and an anonymous referee for helpful comments.

REFERENCES

- Abraham, Z., & Falceta-Gonçalves, D. 2007, MNRAS, 378, 309
 Abraham, Z., Falceta-Gonçalves, D., & Beaklini, P. P. B. 2014, ApJ, 791, 95
 Abraham, Z., Falceta-Gonçalves, D., Dominici, T. P., Nyman L.-A. D. P., McAuliffe F., Caproni A., Jatenco-Pereira V. 2005, A&A, 437, 977
 Akashi, M. S., Kashi, A., & Soker, N. 2013, NewA, 18, 23
 Akashi, M., Soker, N., & Behar, E. 2006, ApJ, 644, 451
 Brott, I., de Mink, S. E., Cantiello, M., et al. 2011, A&A, 530, A115
 Clementel, N., Madura, T. I., Kruij, C. J. H., & Paardekooper, J.-P. 2015a, MNRAS, 450, 1388
 Clementel, N., Madura, T. I., Kruij, C. J. H., Paardekooper, J.-P., & Gull, T. R. 2015b, MNRAS, 447, 2445
 Corcoran, M. F. 2005, AJ, 129, 2018
 Corcoran, M. F., Hamaguchi, K., Pittard, J. M., Russell, C. M. P., Owocki, S. P., Parkin, E. R., & Okazaki, A. 2010, ApJ, 725, 1528
 Chen, Y., Bressan, A., Girardi, L., et al. 2015, MNRAS, 452, 1068
 Crowther, P. A., & Bohannan, B. 1997, A&A, 317, 532
 Damineli, A. 1996, ApJL, 460, L49
 Damineli, A., Conti, P. S., & Lopes, D. F. 1997, NewA, 2, 107
 Damineli, A., Hillier, D. J., Corcoran, M. F., et al. 2008a, MNRAS, 384, 1649
 Damineli, A., Hillier, D. J., Corcoran, M. F., Stahl O., Groh J. H., Arias J., Teodoro M., & Morrell N. 2008b, MNRAS, 386, 2330
 Davidson, K., Dufour, R. J., Walborn, N. R., & Gull, T. R. 1986, ApJ, 305, 867
 Davidson, K., Martin, J., Humphreys, R. M., et al. 2005, AJ, 129, 900
 Davidson, K., & Humphreys, R. M. 1997, ARA&A, 35, 1
 Davidson, K., Mehner, A., Humphreys, R. M., Martin, J. C., & Ishibashi, K. 2015, ApJL, 801, L15
 Dufour, R. J., Glover, T. W., Hester, J. J., et al. 1997, Luminous Blue Variables: Massive Stars in Transition, 120, 255
 Duncan, R. A., & White, S. M. 2003, MNRAS, 338, 425
 Ekström, S., Georgy, C., Eggenberger, P., et al. 2012, A&A, 537, A146
 Falceta-Gonçalves, D., Abraham, Z., & Jatenco-Pereira, V. 2007, IAU Symposium, 240, 198
 Falceta-Gonçalves, D., Jatenco-Pereira, V., & Abraham, Z. 2005, MNRAS, 357, 895
 Figer, D. F., Najarro, F., Morris, M., McLean, I. S., Geballe, T. R., Ghez, A. M., & Langer, N. 1998, ApJ, 506, 384
 Georgy, C., Ekström, S., Meynet, G., et al. 2012, A&A, 542, A29
 Gomez, H. L., Vlahakis, C., Stretch, C. M., Dunne, L., Eales, S. A., Beelen, A., Gomez, E. L., & Edmunds, M. G. 2010, MNRAS, 401, L48
 Groh, J. H., Hillier, D. J., Madura, T. I., & Weigelt, G. 2012, MNRAS, 423, 1623
 Groh, J. H., Nielsen, K. E., Damineli, A., et al. 2010, A&A, 517, A9
 Grunhut, J. H., Wade, G. A., Leutenegger, M., et al. 2013, MNRAS, 428, 1686
 Gull, T. R., Madura, T. I., Groh, J. H., & Corcoran, M. F. 2011, ApJL, 743, L3
 Hamaguchi, K., Corcoran, M. F., Gull, T., et al. 2007, ApJ, 663, 522
 Hamaguchi, K., Corcoran, M. F., Russell, C. M. P., et al. 2014a, ApJ, 784, 125
 Hamaguchi, K., Corcoran, M. F., Takahashi, H., et al. 2014b, ApJ, 795, 119

- Henley, D. B., Corcoran, M. F., Pittard, J. M., et al. 2008, *ApJ*, 680, 705
- Hillier, D. J., Davidson, K., Ishibashi, K., & Gull, T. 2001, *ApJ*, 553, 837
- Humphreys, R. M., Davidson, K., & Koppelman, M. 2008, *AJ*, 135, 1249
- Iping, R. C., Sonneborn, G., Gull, T. R., Massa, D. L., & Hillier, D. J. 2005, *ApJL*, 633, L37
- Kashi, A., Davidson, K., & Humphreys, R. M. 2016, *ApJ*, 817, 66
- Kashi, A., & Soker, N. 2007, *NewA*, 12, 590
- Kashi, A., & Soker, N. 2008, *MNRAS*, 390, 1751
- Kashi, A., & Soker, N. 2009a, *ApJL*, 701, L59
- Kashi, A., & Soker, N. 2009b, *MNRAS*, 397, 1426
- Kashi, A., & Soker, N. 2009, *NewA*, 14, 11
- Kashi, A., & Soker, N. 2010a, *ApJ*, 723, 602
- Kashi, A., & Soker, N. 2010b, *arXiv:1011.1222*
- Kashi, A., & Soker, N. 2011, *arXiv:1104.4655*
- Kashi, A., & Soker, N. 2015, *RAA*, (*arXiv:1508.00004*)
- Köhler, K., Langer, N., de Koter, A., et al. 2015, *A&A*, 573, A71
- Leuening, U., Hamann, W.-R., & Jeffery, C. S. 1996, *A&A*, 312, 167
- Leuening, U., & Hamann, W.-R. 1998, *A&A*, 330, 265
- Livio, M., & Pringle, J. E. 1998, *MNRAS*, 295, L59
- Madura, T. I., Clementel, N., Gull, T. R., Kruip, C. J. H., & Paardekoooper, J.-P. 2015, *MNRAS*, 449, 3780
- Madura, T. I., Gull, T. R., Okazaki, A. T., Russell, C. M. P., Owocki, S. P., Groh, J. H., Corcoran, M. F., Hamaguchi, K., & Teodoro, M. 2013, *MNRAS*, 436, 3820
- Madura, T. I., Gull, T. R., Owocki, S. P., Groh, J. H., Okazaki, A. T., Russell, C. M. P. 2012, *MNRAS*, 420, 2064
- Matt, S., & Balick, B. 2004, *ApJ*, 615, 921
- Mehner, A., Davidson, K., Ferland, G. J., & Humphreys, R. M. 2010, *ApJ*, 710, 729
- Mehner, A., Davidson, K., & Ferland, G. J. 2011, *ApJ*, 737, 70
- Mehner, A., Davidson, K., Martin, J. C., et al. 2011, *ApJ*, 740, 80
- Mehner, A., Davidson, K., Ferland, G. J., Humphreys, R. M. 2010, *ApJ*, 710, 729
- Martin, J. C., Davidson, K., Humphreys, R. M., & Mehner, A. 2010, *AJ*, 139, 2056
- Mehner, A., Davidson, K., Humphreys, R. M., et al. 2012, *ApJ*, 751, 73
- Mehner, A., Davidson, K., Humphreys, R. M., et al. 2015, *A&A*, 578, A122
- Nielsen, K. E., Corcoran, M. F., Gull, T. R., Hillier, D. J., Hamaguchi, K., Ivarsson, S., & Lindler, D. J. 2007, *ApJ*, 660, 669
- Okazaki, A. T., Owocki, S. P., Russell, C. M. P., & Corcoran, M. F. 2008, *MNRAS*, 388, L39
- Parkin, E. R., Pittard, J. M., Corcoran, M. F., Hamaguchi, K., & Stevens, I. R. 2009, *MNRAS*, 394, 1758
- Pittard, J. M., & Corcoran, M. F. 2002, *A&A*, 383, 636
- Pittard, J. M., Stevens, I. R., Corcoran, M. F., & Ishibashi, K. 1998, *MNRAS*, 299, L5
- Portegies Zwart, S. F., & van den Heuvel, E. P. J. 2016, *MNRAS*, 456, 3401
- Richardson, N. D., Gies, D. R., Gull, T. R., Moffat, A. F. J., & St-Jean, L. 2015, *arXiv:1507.07417*
- Smith, N. 2006, *ApJ*, 644, 1151
- Smith, N. 2010, *MNRAS*, 402, 145
- Smith, N., & Ferland, G. J. 2007, *ApJ*, 655, 911
- Smith, N., & Frew, D. J. 2011, *MNRAS*, 415, 2009
- Smith, N., Morse, J. A., Davidson, K., & Humphreys, R. M. 2000, *AJ*, 120, 920
- Soker, N. 2005, *ApJ*, 635, 540
- Soker, N. 2001, *MNRAS*, 325, 584
- Teodoro, M., Daminieli, A., Heathcote, B., et al. 2016, *ApJ*, 819, 131
- Tsebrenko, D., Akashi, M., & Soker, N. 2013, *MNRAS*, 429, 294
- Verner, E., Bruhweiler, F., & Gull, T. 2005, *ApJ*, 624, 973
- Weis, K., Stahl, O., Bomans, D. J., et al. 2005, *AJ*, 129, 1694
- Wessolowski, U., Schmutz, W., & Hamann, W.-R. 1988, *A&A*, 194, 160
- Whitelock, P. A., Feast, M. W., Marang, F., & Breedt, E. 2004, *MNRAS*, 352, 447
- Yungelson, L. R., van den Heuvel, E. P. J., Vink, J. S., Portegies Zwart, S. F., & de Koter, A. 2008, *A&A*, 477, 223
- Yusof, N., Hirschi, R., Meynet, G., et al. 2013, *MNRAS*, 433, 1114